JOURNAL OF GEOPHYSICAL RESEARCH, VOL. 94, NO. B9, PAGES 12,483–12,498, SEPTEMBER 10, 1989

Chemical and Isotopic Evolution of the Coastal Batholith of Southern Peru

M. BOILY,[1] C. BROOKS, AND J. N. LUDDEN

Département de Géologie, Université de Montréal, Montréal, Québec, Canada

D. E. JAMES

Department of Terrestrial Magnetism, Carnegie Institution of Washington, Washington, D. C.

Southeast of Arequipa, the Coastal Batholith of southern Peru is composed of two segments (Arequipa and Toquepala) including five superunits which were emplaced in discrete magmatic pulses from the Jurassic to the Paleocene eras (190–61 Ma). Most superunits intruded a Precambrian basement dominated by granulitic and amphibolitic rocks showing a strong enrichment in large ion lithophile elements, low $\varepsilon_{Nd\ p}$ (−21 to −29) and $^{206}Pb/^{204}Pb_p$ (16.11–17.03 (Tilton and Barreiro, 1980)), and high $\varepsilon_{Sr\ p}$ (+396 to +999) values. Major and trace element analyses reveal that each superunit is formed by distinct suites of calc-alkaline plutons (i.e., "I" type) that range in composition from quartz gabbro to monzogranite. For the whole plutonic suite located in southern Peru, the evolution toward negative $\varepsilon_{Nd\ i}$ and positive $\varepsilon_{Sr\ i}$ values is followed by a significant decrease in $^{206}Pb/^{204}Pb_i$ ratios but is also related to the density of Precambrian outcrops. This led us to classify the intrusives into three groups. Group 1 consists of intrusives carrying positive $\varepsilon_{Nd\ i}$ (+2.4 to +0.4) and generally negative $\varepsilon_{Sr\ i}$ values (−7.4 to +0.7). They are located in the Ilo-Moquegua transect (17°22′–17°80′S), an area where Precambrian exposure is scarce. Group 2 consists of plutons with intermediate ε values (i.e., $\varepsilon_{Nd\ i}$ = +0.5 to −2.2 and $\varepsilon_{Sr\ i}$ = +7.1 to +55.7), which are found in the vicinity of Arequipa and Tarata where numerous Precambrian outcrops are present. Finally, group 3 is composed of intrusives showing negative $\varepsilon_{Nd\ i}$ (−4.4 to −8.0) and positive $\varepsilon_{Sr\ i}$ values (+27.1 to +56.1), including one anomalous granodiorite exposed near Tarata and two samples collected in the Arequipa quadrangle near the contact with the Charcani gneiss. There are several petrogenetic models which can explain the trace element, isotopic, and geographic correlations observed within the Coastal Batholith of southern Peru. One simple model advocates that the parental mafic magma(s) of the plutonic suites of each superunit must be ultimately derived from an isotopically depleted mantle wedge above the subduction zone. The gabbro-diorite-granodiorite-monzogranite association is formed via fractional crystallization and crustal assimilation (i.e., AFC) during ascent in the Andean crust. If the exposed Precambrian crust represents a good compositional average of the upper crustal material assimilated, then the isotopic and some of the trace element variations observed in the three groups can be related to various amounts of crustal assimilation (i.e., small for group 1, but substantial for group 3), although surprisingly little assimilation is required when considering all southern Peruvian intrusives. More complex models advocate different parental mafic magmas formed by various mixtures of lower crustal and mantle derived melts, both having heterogenous but depleted Nd and Sr isotopic compositions. The parental magmas would then ascend, differentiate, and assimilate upper crustal materials of different compositions (i.e., a crust similar to the exposed Precambrian basement for groups 2 and 3 and a less enriched crust, not exposed in the area, for group 1). If the first model is correct, then the relatively small degree of crustal assimilation experienced during the formation of the Coastal Batholith of southern Peru is consistent with the hypothesis that the thick Andean crust was thinned during the prevailing extensional tectonic regime that led to the formation of a marginal basin in central Peru during the late Mesozoic. This allowed the basic magmas to encounter the base of the Precambrian section at shallower depth and spend less time ascending and differentiating in this enriched crust, effectively limiting the amount of assimilation.

INTRODUCTION

Voluminous intrusions of calc-alkaline plutons characterize the magmatic processes related to ocean-continent collisions. The Coastal Batholith of southern Peru is a typical example; it forms a continuous linear belt of Late Jurassic to early Tertiary calc-alkaline intrusives related to subduction magmatism and confined to elongated NW-SE basins running parallel to the Peru-Chile trench. Based on gravity and seismic studies conducted by *Couch et al.* [1981] and *Jones* [1981] in northern and central Peru, *Atherton et al.* [1983] suggested that the Coastal Batholith was largely emplaced in an extensional marginal basin formed during the late Mesozoic. Geochemical and isotopic investigations of plutonic rocks in this area clearly point toward a mantle source, with minimal crustal involvement at any stage of their evolution [*Mukasa*, 1986*a*; *Beckinsale et al.*, 1985; *Atherton et al.*, 1979]. However, gravity and seismic profiles in southernmost Peru (17°–18°S [*Jones*, 1981]) depict a crustal section with no fossil marginal basin; instead it is replaced by a slab of low density crust (2.75 g/cm^3) probably representing the Precambrian-Paleozoic craton (the Arequipa Massif [*Shackleton et al.*, 1979]). This would suggest that the formation of the southern part of the Peruvian Coastal Batholith has been greatly influenced by an old crustal segment.

While the northern and central Peruvian segments (Lima and Trujillo) have been extensively studied, less attention

[1]Now at Institut de Recherche et d'Exploration Miniere/Mineral Exploration Research Institute, Ecole Polytechnique, Montréal, Québec, Canada.

Paper number 89JB00775.
0148-0227/89/89JB-00775$05.00

has been devoted to the Arequipa and Toquepala segments exposed in southern Peru between Arequipa and Tacna. New U-Pb and Rb-Sr ages were recently reported for most superunits [see *Beckinsale et al.*, 1985; *Mukasa*, 1986*b*], but no geochemical investigation combining major and trace elements with radiogenic isotopes has been completed prior to this study. For this purpose, we have analyzed a wide spectrum of rock types, ranging from gabbro to granodiorite, in each of the five superunits that constitute the Toquepala and Arequipa segments. Our principal goal is to understand better the chemical evolution of an unusual portion of the Coastal Batholith largely emplaced in a Precambrian basement.

GEOLOGICAL AND GEOCHRONOLOGICAL BACKGROUND

Cobbing et al. [1977] and *Cobbing and Pitcher* [1983] have subdivided the 2000 × 60 km Peruvian Coastal Batholith into five segments: starting in the northeast with the Piura segment (5°S) and evolving progressively southeastward through the Trujillo, Lima, Arequipa, and Toquepala segments (17°S). Each segment is divided in cohesive superunits which form the basis of their classification. Superunits define consistent spatial and temporal associations of plutons showing progressive evolution of both mineralogy and texture [*Cobbing and Pitcher*, 1983; *Atherton et al.*, 197?]. They are composed of a family of rock types (from quartz-gabbro to monzogranite) apparently defining consanguineous magma series that evolve from basic to siliceous compositions with decreasing intrusive ages.

In southern Peru the Coastal Batholith per se is exposed along the Pacific coastline (Figure 1). *Cobbing and Pitcher* [1983] and later *Beckinsale et al.* [1985] grouped these coastal plutons under two superunits: Ilo and Punta Coles, which form part of the Toquepala segment extending from Arequipa to Tacna. U-Pb age determinations conducted by *Mukasa* [1986*b*] and K-Ar and Rb-Sr mineral/whole rock dating by *Beckinsale et al.* [1985] gave a range of 184–190 Ma for the Punta Coles superunit and of 99–111 Ma for the Ilo superunit. The distribution of the Punta Coles intrusives is patchy. Some plutons occur as discrete gabbroic-dioritic bodies along the coast and intrude Jurassic volcanic rocks of the Chocolate and Guaneros formations [*Garcia*, 1968] or in rare instances cut through Precambrian gneiss. The Ilo superunit crops out farther inland and also cuts through the Jurassic volcanic and plutonic sequences. To the east, the plutons are often covered by sediments of the Moquegua Formation or by the Toquepala group volcanics. The intrusives form either large linear complex units or discrete stocks whose compositions range from tonalite to granodiorite [*Pitcher*, 1985].

The eastern branch of the southern Coastal Batholith extends from Arequipa to the Chilean border. *Pitcher* [1985] and *Beckinsale et al.* [1985] included these "elongated steep-walled flat roofed complex plutons" in the Linga-Yarabamba superunit. U-Pb zircon dating by *Mukasa* [1986*b*] for the northern end-members combined with Rb-Sr and K-Ar age determinations by *Beckinsale et al.* [1985] and *Stewart et al.* [1974] for plutons lying farther south, yield ages of 59–67 Ma (i.e., late Cretaceous to early Paleocene). A variety of rock types ranging from quartz-monzodiorite to monzogranite compose this super-unit [*Pitcher*, 1985]. Near Arequipa, the Linga-Yarabamba plutons clearly cut through Precambrian gneiss and older intrusives of the Arequipa segment. They also intrude the Late Jurassic–Early Cretaceous Yura Group but are in turn overlain by Pliocene ignimbrites of the Sencca Formation. To the southeast, the intrusives outcrop only sparsely through the Chocolate Formation and in some places through the oldest formations of the Toquepala Group, but are generally overlain by the latter.

The Tiabaya and Linga-Arequipa superunits form the southern tip of the Arequipa segment. The Late Cretaceous Tiabaya intrusives (78–86 Ma from U-Pb zircon dating by *Mukasa* [1986*b*] and K-Ar age determinations by *Stewart et al.* [1974] and *Moore* [1984]) are composed of monzogabbros, quartz-monzodiorites and granodiorites. Although we have extensively sampled the Tiabaya superunit, few samples were collected from the adjacent Linga-Arequipa superunit which chiefly consists of monzogabbroic to monzogranitic rocks characterized by pink K-feldspars [*Pitcher*, 1985]. U-Pb, K-Ar, and Rb-Sr dating by *Mukasa* [1986*a*] and *Beckinsale et al.* [1985] indicate younger ages for this superunit than for the adjacent Linga-Ica superunit (i.e., 61–71 Ma versus 96–101 Ma), despite similar bulk composition. Both the Linga-Arequipa and Tiabaya superunits outcrop next to or intrude Precambrian gneiss and cut through Jurassic to Lower Cretaceous volcanics and sediments of the Chocolate Formation and Yura Group. They also intrude early gabbroic sequences which are believe to represent the precursors of the Coastal Batholith. Early Pliocene ignimbrites of the Sencca Formation overlie the Tiabaya superunit on its western edge.

CHEMICAL COMPOSITION OF THE SOUTHERN COASTAL BATHOLITH OF PERU

Analytical Procedures

Major element analyses were acquired with a semiautomated Phillips X ray spectrometer on glass pellets prepared according to the procedure of *Norrich and Hutton* [1969]. Calibration curves for each element were carefully established with selected U.S. Geological Survey (USGS) standards, and the Fe_2O_3/FeO ratio was calculated using the method given by *LeMaître* [1976]. H_2O^+ and CO_2 determinations were obtained by gas chromatography on small aliquots of rock powder (100–200 mg) previously dried at 150°C for 30 min in a vacuum oven. Repeated analyses of internal CO_2 and H_2O standards were made to ensure good calibration and reproductibility.

The trace elements Ba, Rb, Sr, Y, Nb, Zr, Ni, Cr, and V were subsequently determined on pressed powder pellets with a fully automated Phillips PW-1410 X ray spectrometer. Calibration curves for each element were established with various USGS, Centre de Recherches Petrographiques et Geochimiques (CRPG), and Bureau de Recherches Geologiques et Minieres (BRGM) standards and corrections for secondary mass absorption were either calculated via the Mo Compton scatter peak or directly from the available major element data. To check for reproductibility and precision, USGS standards were recycled overnight through the course of this study. In general, the given analytical precision based on counting statistics is 10–15% for Ba, Y, Ni, Cr, and V; 5% for Nb, and 2–5% for Rb, Sr, and Zr. Special care was taken to obtain Rb and Sr determinations for all samples later analyzed for their Sr isotopic composition. For these, repeated analyses ($n > 10$) were carried out with long

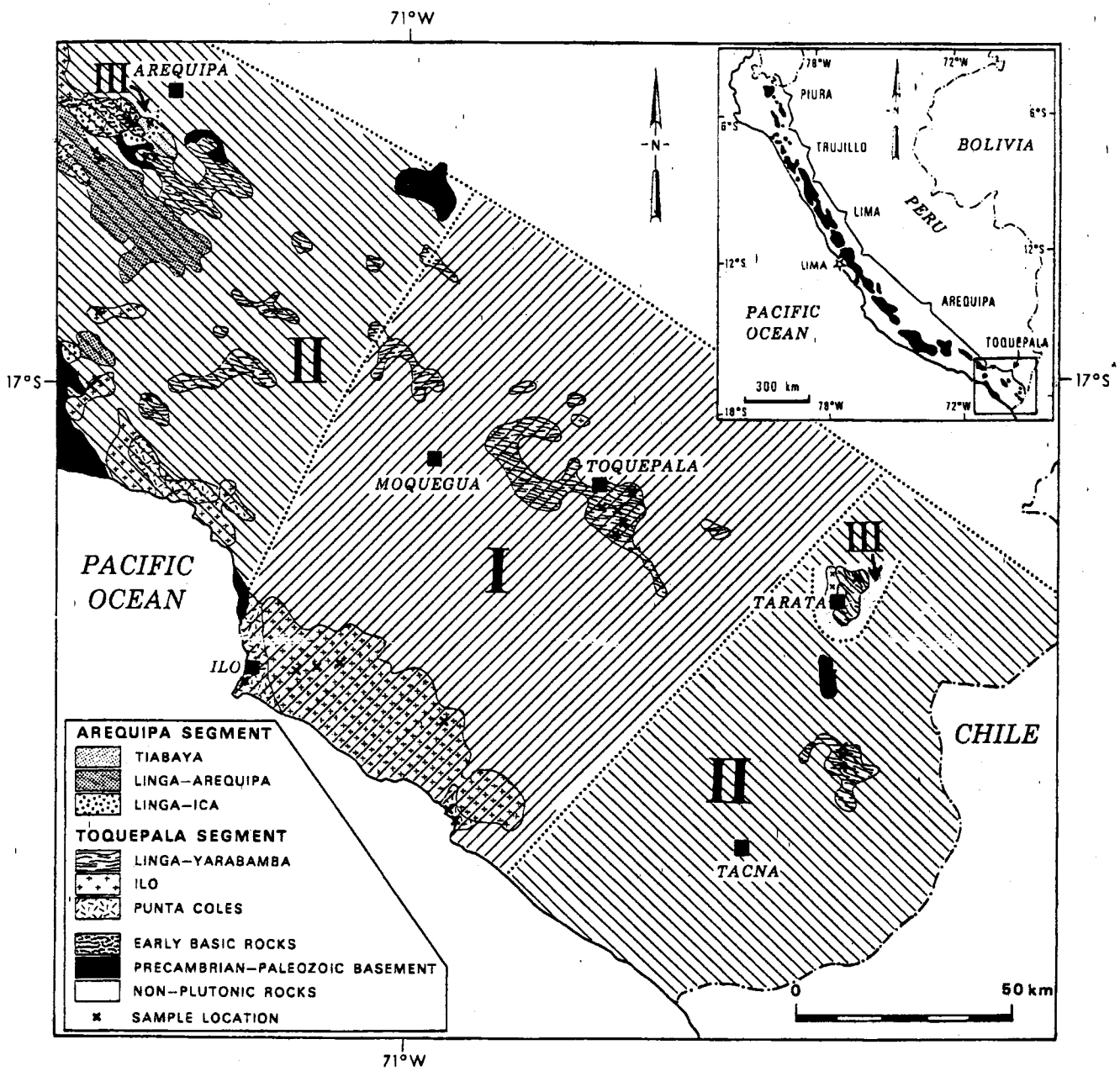

Fig. 1. Geologic map of southwestern Peru showing the exposed superunits of the Arequipa and Toquepala segments. I, II (i.e., the Ilo-Moquegua transect), and III represent the specific fields of each group as defined by the Nd and Sr isotopic signatures of the intrusives and the density of Precambrian outcrops (see text). The hatching emphasizes the boundaries defined by groups I and II. Modified after *Pitcher* [1985] and *Moore* [1984].

counting time on peak and background positions. This allowed the improvement of the analytical precision to better than 1 and 2% for Sr and Rb, respectively ($1\sigma_m$).

The concentration of the rare earth elements (La, Ce, Nd, Sm, Tb, Ho, Tm, Yb, and Lu) and other trace elements (Ta, Hf, Th, U, Sc, and Co) were obtained via the instrumental neutron activation analysis (INAA) technique. For each sample, 1–2 g of rock powder were weighed and sealed in a clean polyethylene vial and irradiated for 2 hours at a constant flux of 10^{12} neutrons cm^{-1} s^{-1} in a SLOWPOKE reactor located at the Ecole Polytechnique de Montréal. The samples were left to cool for 5 days before being counted alternatively on two detectors: an ORTEC Low Energy Photon Scintillaton planar detector (LEPS) and a APTEC/NRD Ge(Li) co-axial detector both wired to a Canberra Multichannel analyzer (MCA) and IBM PC for data collection and reduction. In general, a complete analysis for one sample required five counting periods lasting 10,000 to 50,000 s and extending from 5 to 60 days after irradiation. Precision based on counting statistics is 2–5% for La, Sm, Eu, and Sc; 5–10% for Ce, Yb, Lu, Ta, Hf, and Co; and 10–20% for Tb, Tm, Th, and U. Moreover, great care was exercised in getting high precision determinations for all Nd and Sm concentrations so we could compare the INAA results with those obtained by the isotopic dilution technique. However, since ^{147}Nd is also a fission product of ^{235}U and due to spectral interferences produced by ^{233}Pa and ^{239}Np at 103.1 and 103.3 keV under the ^{153}Sm peak (103.1 keV), the analytical precision can vary between 1 and 5% and 6 and 12% for Sm and Nd, respectively ($1\sigma_m$).

For Nd and Sr isotopic analyses, 100–300 mg of rock powder were weighed into a 10-mL teflon beaker and left to decompose in a HF-$HClO_4$ (4 : 1) mixture for 24 hours at room temperature. After evaporation to dryness on a hot plate, the residue was dissolved in a hot (100°C) 6.2 *N* HCl solution. Usually at this stage we often observed undissolved specks sitting at the bottom of the beaker or flotting in the solution. Therefore, to ensure a complete dissolution, the whole solution was transferred into a 15-mL polypropylene tube, and after repeated centrifuging and decantation, the residue and precipitate were then poured into a teflon bomb in a HF-HNO_3 mixture (10 : 1). The remaining liquid was then poured back into the tube and kept for further use. The bomb was sealed in a stainless steel jacket and left in the oven at 200°C for 4–5 days. Usually after this step, we obtained a clear solution devoid of any visible residue. Following evaporation on a hot plate, the bomb precipitate was then taken in 6.2 *N* HCl and mixed with the solution sitting in the polypropylene tube. The last step involved the dissolution of the whole sample in 2.5 *N* HCl. This technique was slightly modified for spiked samples. After directly spiking the solid in a teflon beaker with an enriched ^{150}Nd and ^{149}Sm solution, no decantation and centrifuging were done. Instead, the whole 6.2 *N* HCl solution was directly poured into the teflon bomb after the HF-$HClO_4$ attack in an open beaker. This step was considered necessary to ensure complete homogenization of spike and sample throughout the dissolution procedure.

Sr elution was performed on a 30 cm × 5 mm pyrex column filled with DOWEX® 50W-X8 cation exchange resin. The analytical procedures closely followed those reported by *Hart and Brooks* [1977]. Usually, 50–100 μL of 2.5 *N* HCl solution were processed twice through the column to ensure Rb free runs and to obtain between 200 and 800 ng of Sr in the mass spectrometer. The rare earth elements (REEs) were collected in a subsequent elution using 2.5 and 6.2 *N* HCl. In general, 500 μL to 1.5 mL of solution were passed through the cationic column in order to obtain 200–600 ng of Nd and 30–60 ng of Sm. Separation of Nd and Sm from the other rare earths was then performed via reverse phase chromatography using an HDEHP-coated teflon medium [see *Zindler et al.*, 1979]. Nd was first eluted with 0.25 *N* HCl followed by Sm with 0.60 *N* HCl.

All isotopic analyses, except when specified, were acquired at the Université de Montréal on a National Bureau of Standards (NBS) 12-inch radius mass spectrometer equipped with a CARY-401 electrometer and attached to a PDP-11 computer and later to an IBM PC. Nd was loaded on a Ta side filament in a 2.5 *N* HCl-0.1 *N* H_3PO_4 (1 : 1) solution and run in a double filament configuration using a center Re filament. The $^{143}Nd/^{144}Nd$ ratios were corrected for mass fractionation using a $^{146}Nd/^{144}Nd$ value of 0.7219. For unspiked runs, we closely monitored the $^{150}Nd/^{146}Nd$ ratios, and a compilation of all determinations made in this laboratory gives an average of 0.327466 ± 18 (n = 26, $2\sigma_m$) which is slightly lower than the values of 0.327494 extrapolated from *Wasserburg et al.* [1981] and of 0.32748 (unpublished Massachusetts Institute of Technology (MIT) value). The ^{147}Sm peak was also monitored to evaluate the contribution of ^{144}Sm under the ^{144}Nd peak. In all cases, it was found to be less than 5 to 10^{-6} of the total $^{143}Nd/^{144}Nd$ value. During the course of this study several analyses of BCR-1 and JMC-321 produced mean values of 0.512644 ± 24 (n = 4, $2\sigma_m$) and 0.511868 ± 18 (n = 14, $2\sigma_m$), respectively. Concentrations of Nd and Sm were also determined on BCR-1, and we report values of 28.788 ppm for Nd and 6.591 ppm for Sm, which are in close agreement with the published values of *Chauvel et al.* [1985]. Nd and Sm concentrations acquired both by INAA and isotope dilution techniques show low but systematic discrepancies, the ID determinations being generally higher by 1% for Nd and by 5–7% for Sm. For the purpose of data homogenization, we corrected the Nd and Sm concentrations obtained via INAA by 1% and 7%, respectively.

TABLE 1. Summary of Major and Trace Element Data

	Arequipa		Toquepala		
	Tiabaya	Linga-Arequipa	Linga-Yarabamba	Ilo	Punta Coles
			Major Elements, wt %		
n	19	3	16	8	3
SiO_2	58.56	58.23	62.10	60.85	54.53
Al_2O_3	17.10	16.62	16.52	16.83	19.00
TiO_2	0.72	0.86	0.69	0.61	0.80
Fe_2O_3	3.56	3.47	2.91	2.80	3.65
FeO	4.61	4.51	3.82	3.65	5.20
MnO	0.16	0.15	0.13	0.21	0.17
MgO	3.03	2.69	2.32	2.55	3.51
CaO	6.51	6.42	5.09	6.36	8.39
Na_2O	3.34	3.78	3.50	3.51	3.46
K_2O	2.22	3.02	2.71	2.53	0.83
P_2O_5	0.19	0.55	0.20	0.19	0.21
H_2O^+	1.24	0.64	1.47	1.28	1.61
CO_2	0.16	0.14	0.17	0.22	0.15
			Trace Elements, ppm		
Ba	683	682	620	514	372
Rb	69.4	139.8	96.6	72.2	64.1
Sr	485.4	521.7	424.4	446.5	367.5
Zr	90.7	161.5	154.6	106.6	132.4
Nb	7.4	9.4	10.3	7.8	7.0
Y	20	25	24	19	25
Ni	14	16	19	13	28
Cr	54	53	64	53	95
V	178	157	116	159	250
La*	20.9	22.8	24.0	16.7	10.3
Ce	42.9	46.8	46.6	35.6	22.8
Nd	21.2	24.1	19.1	17.1	14.8
Sm	3.94	4.57	4.26	3.31	3.03
Eu	1.06	1.03	0.97	0.83	1.06
Tb	0.67	0.85	0.59	0.65	0.72
Ho	0.62	0.84	0.83	0.60	0.60
Tm	0.24	0.27	0.24	0.26	0.30
Yb	1.86	2.09	1.87	1.76	1.71
Lu	0.30	0.34	0.28	0.30	0.33
Ta	1.0	1.8	1.3	1.6	0.7
Hf	2.8	4.6	4.2	3.1	2.5
Th	8	24	10	8	1
U	1.5	5.7	2.3	2.1	0.4
Sc	19.64	16.20	13.87	15.55	24.67
Co	35.6	46.6	32.4	40.3	36.7
Rb/Sr	0.14	0.27	0.23	0.16	0.17
Zr/Nb	12.3	7.3	15.0	13.6	18.9
Zr/Y	4.5	6.4	6.6	5.6	5.3
La/Sm	5.3	5.0	5.6	5.0	3.4
La/Yb	11.2	10.9	12.8	9.5	6.0
Th/U	5.4	4.3	4.7	3.9	3.2

*For all rare earth elements and Ta, Hf, Th, U, Sc, and Co; Tiabaya, n = 11; Linga-Arequipa, n = 2; Linga-Yarabamba; n = 9; Ilo, n = 7; Punta Coles, n = 2.

TABLE 2. Rock Type and Sample Location

Sample	Rock Type	Superunit	Latitude S	Longitude W
PE-13	monzogabbro	Tiabaya	15°45.5′	74°24.0′
PE-15	monzodiorite	Tiabaya	16°24.6′	71°39.2′
PE-16	granodiorite	Tiabaya	16°26.3′	71°41.0′
PE-17	quartz-diorite	Tiabaya	16°27.4′	71°41.3′
PE-20	monzodiorite	Tiabaya	17°00.1′	72°02.3′
PE-31	granodiorite	Tiabaya	16°27.0′	71°36.9′
PE-32	granodiorite	Tiabaya	16°27.2′	71°37.3′
PE-33	granodiorite	Tiabaya	16°27.6′	71°37.3′
PE-35	monzogabbro	Tiabaya	16°28.9′	71°36.5′
PE-39	quartz-monzodiorite	Linga-Yarabamba	16°31.8′	71°35.3′
PE-40	quartz-monzodiorite	Linga-Yarabamba	16°31.8′	71°35.3′
PE-41	granodiorite	Linga-Yarabamba	16°31.8′	71°35.3′
PE-42	granodiorite	Linga-Yarabamba	16°31.75′	71°35.3′
PE-43	monzodiorite	Linga-Yarabamba	16°30.9′	71°35.6′
PE-50	granodiorite	Ilo	16°54.3′	71°43.3′
PE-57	granodiorite	Ilo	17°00.8′	71°41.4′
PE-58	quartz-monzodiorite	Ilo	17°01.2′	71°40.6′
PE-59	monzonite	Ilo	17°11.8′	71°04.8′
PE-84	quartz-monzodiorite	Linga-Arequipa	16°31.0′	71°45.3′
PE-85	diorite	Linga-Arequipa	16°31.0′	71°44.7′
PE-86	granodiorite/monzogranite	Linga-Arequipa	16°30.3′	71°44.4′
PE-87	monzodiorite?	Tiabaya	16°29.3′	71°42.6′
PE-88	monzodiorite	Tiabaya	16°29.0′	71°42.5′
PE-89	monzodiorite	Tiabaya	16°29.0′	71°42.5′
PE-90	quartz-monzodiorite	Tiabaya	16°28.8′	71°42.5′
PE-91	quartz-monzodiorite	Tiabaya	16°28.5′	71°42.5′
PE-92	monzodiorite	Tiabaya	16°28.1′	71°41.8′
PE-93	quartz-monzodiorite	Tiabaya	16°28.1′	71°41.8′
PE-94	granodiorite	Tiabaya	16°28.1′	71°41.8′
PE-95	monzodiorite	Tiabaya	16°25.3′	71°41.2′
PE-96	granodiorite	Tiabaya	16°25.3′	71°41.1′
PE-124	monzogranite	Linga-Yarabamba	17°37.0′	70°03.4′
PE-127	granodiorite	Linga-Yarabamba	17°26.5′	70°01.4′
PE-150	granodiorite	Linga-Yarabamba	17°50.3′	70°02.3′
PE-151	granodiorite	Linga-Yarabamba	17°50.0′	70°01.6′
PE-152	quartz-monzodiorite	Linga-Yarabamba	17°50.0′	70°01.6′
PE-154	monzogabbro	Linga-Yarabamba	17°49.1′	70°00.9′
PE-162	quartz-diorite	Punta Coles	17°53′	70°59′
PE-163	quartz-diorite	Punta Coles	17°53.6′	70°57.7′
PE-164	quartz-diorite	Ilo	17°46.1′	71°54.7′
PE-165	quartz-diorite	Ilo	17°36.7′	71°09.9′
PE-166	granodiorite/tonalite	Ilo	17°37.3′	71°10.9′
PE-167	granodiorite/tonalite	Ilo	17°37.8′	71°11.8′
PE-168	quartz-diorite	Punta Coles	17°39.1′	71°20.2′
PE-171	quartz-monzogabbro	Linga-Yarabamba	17°17.5′	70°42.0′
PE-172	quartz-monzodiorite	Linga-Yarabamba	17°17′	70°42′
PE-173	granodiorite	Linga-Yarabamba	17°13.2′	70°37.2′
PE-174	quartz-monzodiorite	Linga-Yarabamba	17°13′	70°39′
PE-185	granodiorite	Linga-Yarabamba	17°15′	70°43′

Sr was taken in TAFPH (a solution of H_3PO_4, H_2O, $TaCl_5$, and HF) and deposited on a W filament. The $^{87}Sr/^{86}Sr$ values were corrected for mass fractionation using a $^{86}Sr/^{88}Sr$ ratio of 0.1194 and normalized to an Eimer and Amend strontium carbonate value of 0.70800. Careful on line monitoring of ^{85}Rb was carried out to evaluate the contribution of ^{87}Rb under the ^{87}Sr peak, and in all cases it was found to be less than 1×10^{-5} of the $^{87}Sr/^{86}Sr$ value. During the course of this study, routine determinations of the E&A standard gave an average $^{87}Sr/^{86}Sr$ value of 0.70784 ± 3 ($n = 10$, $2\sigma_m$). Total procedural blanks for Sr, Nd, and Sm were 0.3, 0.2, and 0.1 ng, respectively, and were considered negligible.

Major and Trace Element Data

A summary of the major and trace element data is given in Table 1 with the sample location and rock type provided in Table 2. The full analytical results can be obtained on request from the senior author. The calc-alkaline affinity of the southern Peruvian Coastal Batholith is clearly demonstrated in the AFM ($A = Na_2O + K_2O$, $F = FeO_T$, $M = MgO$) diagram (Figures 2*a* and 2*b*) in which there is considerable overlap between the five superunits. Table 3 compares the major and trace element chemistry of the intrusives to that of other circum-Pacific granitoids associated with subduction magmatism (the "I" type granitoids; Table 3). Relative to the average western U.S. or northern Chilean coastal batholiths, each superunit is generally less siliceous (54.6–62.1 versus 66% SiO_2 (wt %)); shows a definite enrichment in Cr, V, Co, and Sc; and seems to be slightly depleted in Rb and La. Although there are large variations in their trace element ratios, the southern Peruvian superunits present lower average La/Yb (6.0–12.8 versus 11.1–51.5) and

perhaps slightly lower mean Rb/Sr (0.14–0.27 versus 0.17–0.45) ratios, which is consistent with their less evolved nature. Superunits of the southern Arequipa and Toquepala segments also display comparable major and trace element compositions to some of the voluminous granitoid superunits of the Lima segment generated during the Middle to Late Cretaceous eras [*McCourt*, 1981; *Atherton et al.*, 1979]. The southern Peruvian segments differ however from their northern counterparts through the abundance of mafic to intermediate plutonic rocks (i.e., between 52 and 55 SiO_2 (wt %)) and the absence of superunits dominated by monzogranites.

The chemical evolution of each superunit shows a progressive and predictable enrichment in incompatible elements (i.e., K_2O, Rb, Ba, La, Th) and in certain trace element ratios (i.e., Rb/Sr, La/Yb) with increasing SiO_2 weight percent content (Figure 3). This is generally accompanied by decreasing abundances in compatible elements (Ni, Cr, V, Sc and Co). Chondrite-normalized REE patterns also exhibit enrichment in light REE (LREE), flat heavy REE (HREE) patterns, and negative Eu anomalies in the more evolved plutons (Figure 4). Overall, the most important feature in the chemical evolution of the southern Peruvian Coastal Batholith is that despite showing large variations in their isotopic compositions (see below) and perhaps being emplaced in crustal segments of different age and composition, the five super-units seem to define overlapping and continuous trends in most trace element and major element plots.

There are, however, small but significant chemical differences between each superunit. The Punta Coles superunit, for example, carries relatively low abundances in large ion lithophile element (LILE) and higher concentrations in Cr, V, Sc, and Ni, evidently reflecting its dominant gabbroic/dioritic composition. The oldest superunits, Ilo and Punta Coles, are also slightly more depleted in REE and Ba compared to the intrusives of the younger Cretaceous-Paleocene superunits, the Tiabaya and Linga-Yarabamba being the most enriched.

Nd and Sr Isotopes

Nd and Sr isotopic determinations are reported in Table 4 along with Rb, Sr, Sm, and Nd concentrations. The isotopic measurements were carried out on selected samples covering a wide spectrum of rock types collected from each superunit. We rejected samples showing pronounced signs of alteration; however, we failed to collect fresh gabbroic or dioritic samples in the vicinity of Arequipa, since they seem to have suffered extensive plagioclase sericitization and/or intense chloritization of biotites and secondary amphibole crystallization. We did analyze some gabbros and diorites to get reliable Nd isotopic compositions and to check for possible effects of alteration on $^{87}Sr/^{86}Sr$ initial ratios.

With the exception of three Linga-Yarabamba intrusives (PE-42, PE-43 and PE-127), the isotopic data show a narrow range of $\varepsilon_{Nd\ i}$ values (+2.4 to −2.2). The Sr isotopes display a wider range of positive and negative values (i.e., $\varepsilon_{Sr\ i}$ = −7.4 to +55.7), but if two Tiabaya samples (PE-32 and PE-87, the latter being strongly altered) are excluded along with the Linga-Yarabamba intrusives mentioned above, the range is narrowed to −7.4 to +16.6 (Figure 5).

A crude correlation seems to exist between the age of eruption and isotopic enrichment of the southern Peruvian volcanics, the Cenozoic to Recent ignimbrites and andesites showing the highest enrichment in Nd and Sr, with the

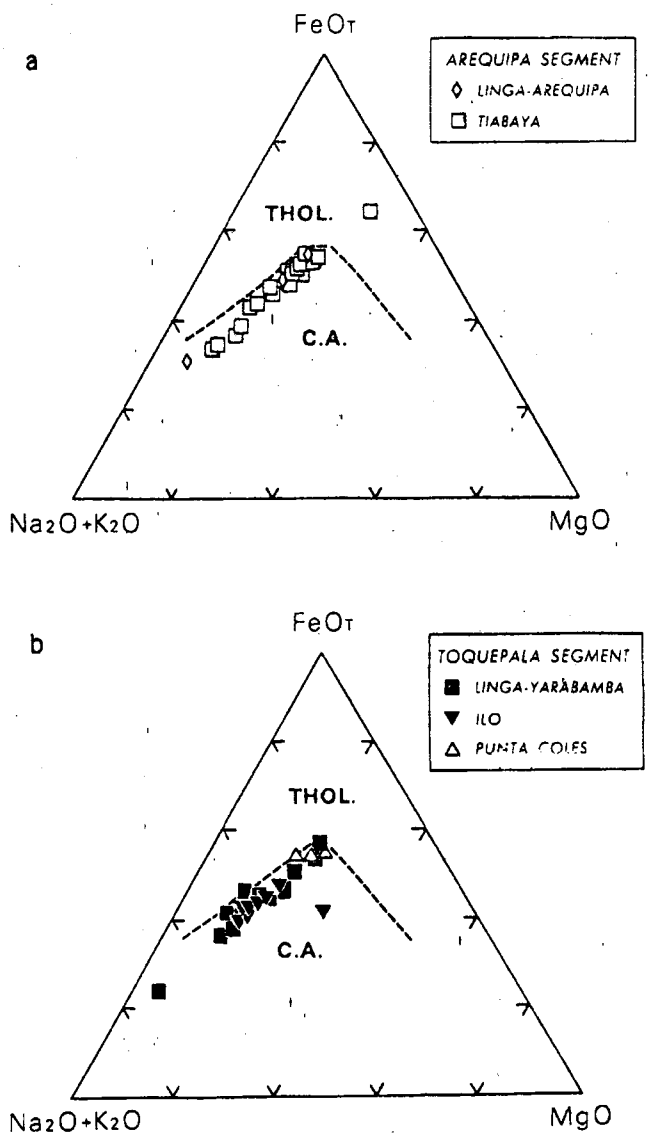

Fig. 2. AFM diagram showing the calc-alkaline affinities and overlapping trends of all superunits. The dashed line represents the boundary for tholeitic (Thol.) and calk-alkaline (C.A.) field of *Irvine and Baragar* [1971].

Jurassic volcanics exposed along the coast being the most depleted (M. Boily et al., Chemical constraints on the evolution of the pre- and post-Oligocene volcanism of southern Peru, submitted to *Geological Society of America Bulletin*, 1989) However, this relationship breaks down for the southern Coastal Batholith. Instead, regardless of their age of emplacement or superunit association, the plutons are rather more easily grouped according to their Nd and Sr isotopic composition and the density of Precambrian outcrops.

The first group (group 1) includes Jurassic to Middle Cretaceous plutons lying along the coast near Ilo (Ilo and Punta Coles superunits) and all Late Cretaceous to early Paleocene Linga-Yarabamba intrusives outcropping near Toquepala. They display positive $\varepsilon_{Nd\ i}$ (+2.4 to +0.4) and negative or slightly positive $\varepsilon_{Sr\ i}$ (−7.4 to + 0.7) values. Although they were probably intruded in a Precambrian basement, they lie in an NNW-SSE transect located between 17°22′ and 17°80°S (the Ilo-Moquegua transect, Figure 1)

TABLE 3. Comparison of the Average Major and Trace Element Content of Plutons Collected in the Five Superunits Forming the Southern Coastal Batholith of Peru and of Other Circum-Pacific Calc-Alkaline Intrusives

				Coastal Batholith of Southern Peru				
				Arequipa Segment		Toquepala Segment		
	Circum-Pacific Average	Sierra Nevada Batholith	Central Chilean Batholith	Tiabaya (n = 19)	Linga-Arequipa (n = 3)	Linga-Yarabamba (n = 16)	Punta Coles (n = 8)	Ilo (n = 3)
				Weight Percent				
SiO_2	66.9	...	65.6	58.56	58.23	62.10	60.85	54.53
K_2O	3.07	3.02	2.94	2.22	3.02	2.71	2.53	0.83
				Parts per Million				
Ba	500	1000	588	683	682	620	514	372
Rb	110	118	110	69.4	139.8	96.6	72.2	64.1
Sr	440	500	611	485.5	521.7	424.4	446.5	367.5
Ni	15	15	10	20	25	24	19	25
Cr	30	30	29	54	53	64	53	95
V	75	100	117	178	157	116	159	250
La	36	30	20	20.9	22.8	24.0	16.7	10.3
Yb	3.6	1.5	1.3	1.86	2.09	1.87	1.76	1.71
Th	10	14.4	11	8	24	10	8	1
U	2.7	4.3	3.5	1.5	5.7	2.3	2.1	0.4
Sc	14	10	9.3	19.6	16.2	13.9	15.6	24.7
Co	10	10	10.1	36	47	32	40	37
Rb/Sr	0.25	0.24	0.17	0.14	0.27	0.23	0.16	0.17
La/Yb	10	20	16	11	11	13	10	6
Th/U	3.7	3.1	3.1	5	4	5	4	3

Data for the Chilean Coastal Batholith, the Sierra Nevada, and the circum-Pacific average are taken from Table 3 of *Lopez-Escobar et al.* [1979].

where Precambrian outcrops are virtually absent. This transect was also subjected to basaltic and andesitic volcanism along the coast in the Late Jurassic (Chocolate and Guaneros Formations [*Boily et al.*, 1984]) and to intense inland andesitic-rhyolitic activity during the Cretaceous-Paleocene eras (i.e., Toquepala Group). It is revealing that these volcanics also present "depleted" characteristics with $\varepsilon_{Sr\,i}$ and $\varepsilon_{Nd\,i}$ values ranging from −13.9 to +15.2 and +7.2 to +0.6, respectively [*James et al.*, 1974; *Boily et al.*, 1984, submitted manuscript, 1989].

A second group (group 2) comprises Late Cretaceous to early Paleocene granitoids intruded in the vicinity of Arequipa (Tiabaya, Linga-Arequipa, and Linga-Yarabamba superunits) and four Linga-Yarabamba intrusives located between Tacna and Tarata. They display a narrow range of $\varepsilon_{Nd\,i}$ values (+0.5 to −2.2) with variable signatures in Sr isotopes ($\varepsilon_{Sr\,i}$ = −7.1 to +55.7). In general, these plutons lie

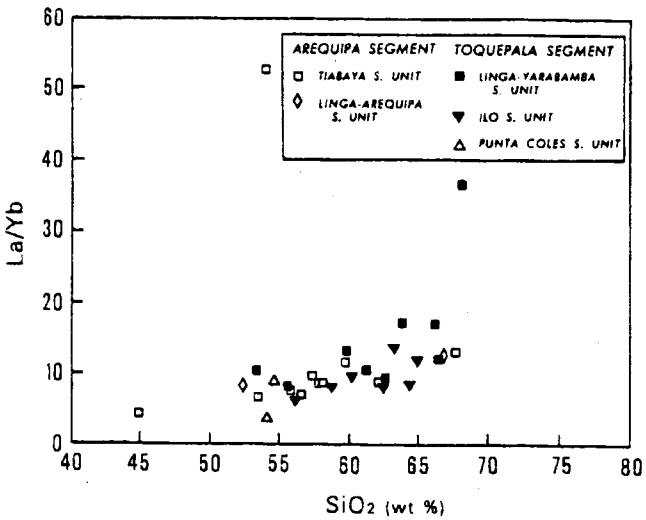

Fig. 3. La/Yb versus SiO_2 (wt %) plot showing the smooth increase of La/Yb ratios with differentiation and the overlapping trend defined by the intrusives of the five superunits.

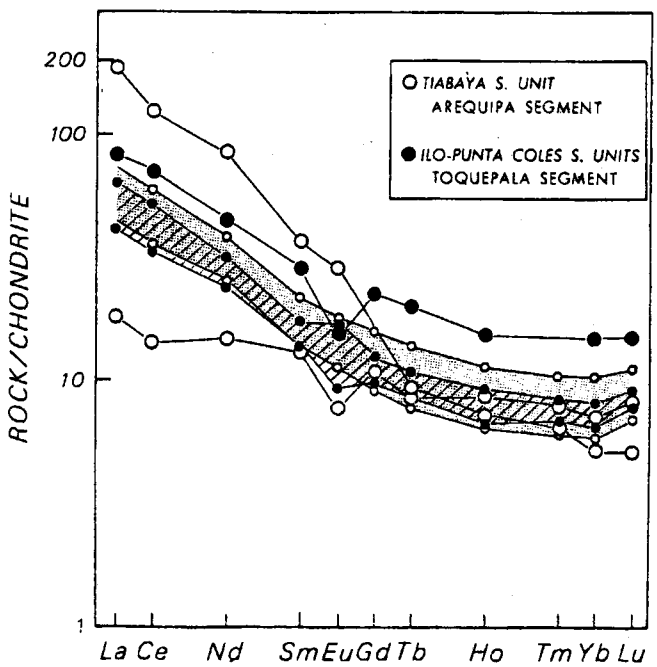

Fig. 4. Chondrite-normalized REE diagram of typical calk-alkaline intrusives collected from the Tiabaya, Ilo, and Punta Coles superunits. Dotted pattern represents the range defined by most Tiabaya plutons (n = 9) and the oblique hatching; the range of most Ilo-Punta Coles intrusives (n = 8).

TABLE 4. Sr and Nd Isotopic Analyses and Rb, Sr, Sm, and Nd Concentrations of Representative Intrusive Samples Collected in the Five Superunits

	Arequipa							Toquepala		
	Tiabaya					Linga-Arequipa		Ilo		
	PE-32	PE-87	PE-90	PE-92	PE-94	PE-85	PE-86	PE-58	PE-164	PE-165
SiO_2, wt %	67.6	56.5	59.6	53.4	62.0	52.3	66.7	60.1	58.6	56.0
Rb, ppm	71.6	77.5	85.6	40.4	102.4	34.4	290.2	100.2	149.5	7.84
Sr, ppm	266.2	347.6	462.8	512.6	403.8	761.4	241.4	418.3	292.4	451.1
Nd, ppm	20.2	17.8	19.0	16.1	20.1	21.4	27.2	17.1	27.4	9.3
Sm, ppm	3.54	4.00	4.05	3.76	4.38	4.79	5.16	3.51	5.96	2.10
$^{147}Sm/^{144}Nd$	0.106	0.136	0.129	0.141	0.132	0.135	0.115	0.124	0.132	0.050
$^{87}Rb/^{86}Sr$	0.778	0.645	0.535	0.228	0.734	0.131	3.478	0.693	1.497	0.137
$^{87}Sr/^{86}Sr_p$	0.709190 ± 40	0.708053 ± 23	0.706172 ± 27	0.705712 ± 33	0.706216 ± 27	0.705085 ± 28	0.708752 ± 28	0.705894 ± 35	0.706194 ± 24	0.704710 ± 27
$^{143}Nd/^{144}Nd_p$	0.512555 ± 19	0.512558 ± 16	0.512506 ± 28	0.512637 ± 25	0.512492 ± 17	0.512553 ± 25	0.512514 ± 14	0.512533 ± 31	0.512535 ± 24	0.512720 ± 29
$\varepsilon_{Sr\,i}$	+55.7	+41.6	+16.6	+14.9	+14.1	+7.7	+13.4	+7.1	−4.9	+3.7
$\varepsilon_{Nd\,i}$	−0.8	−1.0	−1.9	+0.5	−2.2	−1.2	−1.8	−1.2	−1.2	+2.4

	Toquepala										
	Ilo	Punta Coles		Linga-Yarabamba							
	PE-167	PE-162	PE-168	PE-42	PE-43	PE-127	PE-150	PE-152	PE-171	PE-173	PE-174
SiO_2, wt %	64.2	54.5	54.1	66.0	53.2	67.9	62.4	61.1	55.5	66.2	59.7
Rb, ppm	48.6	18.6	20.2	88.5	44.0	74.2	147.6	142.5	92.7	124.4	56.7
Sr, ppm	488.1	583.7	341.6	431.3	578.8	438.4	292.5	322.0	400.8	424.8	533.3
Nd, ppm	15.7	17.7	11.5	16.6	21.8	19.8	25.5	24.8	24.4	19.4	15.6
Sm, ppm	3.61	3.58	3.01	2.90	4.49	3.72	5.31	6.38	6.28	4.56	4.09
$^{147}Sm/^{144}Nd$	0.139	0.122	0.158	0.106	0.124	0.126	0.126	0.156	0.156	0.142	0.159
$^{87}Rb/^{86}Sr$	0.288	0.092	0.171	0.594	0.220	0.490	1.460	1.280	0.669	0.847	0.308
$^{87}Sr/^{86}Sr_p$	0.704776 ± 25	0.704005 ± 29	0.704446 ± 29	0.706850 ± 42	0.705995 ± 27	0.708483 ± 36	0.706302 ± 30	0.706038 ± 29	0.704874 ± 28	0.705194 ± 29	0.704741 ± 32
$^{143}Nd/^{144}Nd_p$	0.512623 ± 24	0.512654 ± 22	0.512681 ± 21	0.512345 ± 17	0.512383 ± 13	0.512202 ± 25	0.512520 ± 18	0.512525 ± 16	0.512739 ± 16	0.512639 ± 20	0.512674 ± 18
$\varepsilon_{Sr\,i}$	−0.3	−7.4	−4.1	+27.1	+19.6	+51.6	+8.7	+7.1	−1.9	+0.5	+0.7
$\varepsilon_{Nd\,i}$	+0.4	+2.1	+1.7	−5.1	−4.4	−8.0	−1.8	−2.0	+2.2	+0.4	+1.0

Subscript p is present-day ratio; i is initial ratio. Superunit emplacement ages used to correct for radiogenic growth are Punta Coles, 190 Ma; Ilo, 103 Ma; Linga-Yarabamba, 61 Ma; Linga-Arequipa, 68 Ma, and Tiabaya, 78 Ma (ages are from *Mukasa* [1986*a*, *b*], *Beckinsale et al.* [1985], *Moore* [1984], and *Stewart et al.* [1974]). $\varepsilon_{Nd\,i} = 10^4((^{143}Nd/^{144}Nd_{rock}(T)/^{143}Nd/^{144}Nd_{CHUR}(T)) - 1)$, where $^{143}Nd/^{144}Nd_{CHUR} = 0.512640–0.1966\,(e^{\lambda T} - 1)$; $\lambda_{Sm} = 6.54 \times 10^{-12}\ yr^{-1}$; $\varepsilon_{Sr\,i} = 10^4((^{87}Sr/^{86}Sr_{rock}(T)/^{87}Sr/^{86}Sr_{UR}(T)) - 1)$, where $^{87}Sr/^{86}Sr_{UR} = 0.7045–0.0827(e^{\lambda T} - 1)$; $\lambda_{Rb} = 1.42 \times 10^{-11}\ yr^{-1}$; T is age in Ma.

in areas where Precambrian schists and gneiss exposures are most abundant (Figure 1).

Finally, group 3 is less well defined and is formed by three enriched Linga-Yarabamba intrusives (PE-42, PE-43, and PE-127; with $\varepsilon_{Nd\ i} = -4.4$ to -8.0 and $\varepsilon_{Sr\ i} = +27.1$ to $+51.6$). The first two samples were collected near the contact with the Charcani gneiss, a typical granulitic unit of the Precambrian-Paleozoic Arequipa Massif south of Arequipa. The isotopic composition of PE-127, a granodiorite, is somewhat enigmatic since it lies about the same distance from Precambrian exposures as the less enriched Linga-Yarabamba plutons exposed farther south (i.e., PE-150 and PE-152). Nonetheless, it is possible that this sample could belong to another younger intrusive unit.

The isotopic variations described above cannot be related to the timing of superunit emplacement, since the entire Linga-Yarabamba superunit, which includes suites of plutons in each of the three groups, was emplaced in a short time span during the early Paleocene (≈61 Ma [*Mukasa*, 1986*b*; *Beckinsale et al.*, 1985]). Furthermore, this correlation also extends to the Jurassic epoch. The elevated $^{87}Sr/^{86}Sr$ initial values observed in Punta Coles tonalites exposed NW of Arequipa (0.7062–0.70785 [*Beckinsale et al.*, 1985]) are found in an area where the plutons are characterized by low $\varepsilon_{Nd\ i}$ values typical of group 2. This is in sharp contrast with the depleted nature of their Jurassic dioritic-gabbroic counterparts exposed along the coast near Ilo (group 1).

Another significant chemical feature of the Coastal Batholith is shown in Figure 6. Within each of the three observed groups, the plutons define slight variations in $\varepsilon_{Nd\ i}$ values with increasing SiO_2 (wt %) content. However the maximum isotopic variations occur between the less evolved plutons of each group. For instance, variations of 7.3 ε units are observed between the low SiO_2 members of groups 1–3, while the difference observed between the mafic to intermediate members inside each group is only 2.5–3.5 ε units.

Other isotopic determinations conducted in the northern Lima and Arequipa segments are primarily for Sr and Pb, with no reported analyses for Nd isotopes. A compilation of initial $^{87}Sr/^{86}Sr$ ratios made by *Beckinsale et al.* [1985] for the Lima segment reveals a restricted range of typical continental arc values (i.e., 0.7040–0.7043). For some of the superunits, Pb isotopic measurements made by *Mukasa* [1986*a*] show $^{206}Pb/^{204}Pb$ ratios close to or slightly higher than the Nazca plate mid-ocean ridge basalts (MORB) values (18.680–20.803). On the other hand, the Arequipa segment superunits display a wider range of $^{87}Sr/^{86}Sr$ initial values, with some showing a definite crustal input ($^{87}Sr/^{86}Sr$ = 0.70461–0.7084 [*Beckinsale et al.*, 1985]). Moreover, plutons of the Arequipa and Toquepala segments around Arequipa exhibit $^{206}Pb/^{204}Pb$ values that trend definitively toward an old granulitic component (i.e., <18.4 [*Mukasa*, 1986*a*]). These low values generally correlate with the elevated $^{87}Sr/^{86}Sr$ ratios (0.70493–0.70806) reported in this study and by *Beckinsale et al.* [1985] for the Tiabaya, Linga-Arequipa, and Linga-Yarabamba superunits. Very few Pb data are given for the Toquepala segment southeast of Arequipa. The results reported by *Barreiro and Clark* [1984] confirm the more depleted nature of the intrusives lying in the Ilo-Moquegua transect, since the range observed in the $^{206}Pb/^{204}Pb$ ratios (18.521–18.753) falls in the field of the Lima segment intrusives lying to the north [*Mukasa*, 1986*a*].

It would then appear that elevated ε_{Sr} and low ε_{Nd} values (groups 2 and 3) are generally correlated with low $^{206}Pb/^{204}Pb$ ratios. As we have seen, these chemical variations can also be correlated to the density of Precambrian outcrops in the studied area. Therefore it is clear that the chemical evolution of the southern Peruvian Coastal Batholith is strongly influenced by the assimilation of a Precambrian granulitic crust whose isotopic and trace element composition is similar to the that of the exposed granulitic outcrops lying in the Arequipa vicinity or along the Pacific coast (Table 5).

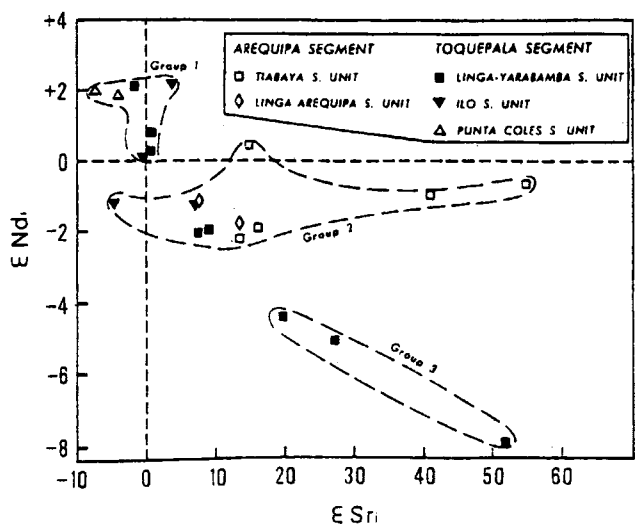

Fig. 5. Initial ε_{Sr} versus ε_{Nd} correlation diagram for the southern Peruvian Coastal Batholith. Three groups are formed according to their isotopic signatures and also in relation to the density of Precambrian exposures in the vicinity of the sampled area (see text).

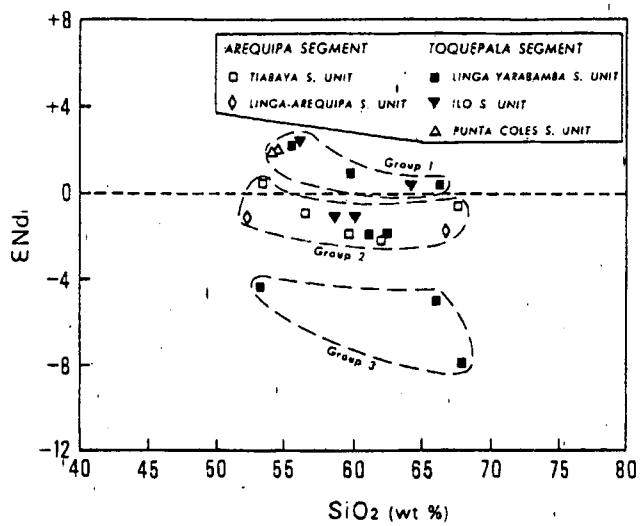

Fig. 6. The $\varepsilon_{Nd\ i}$ versus SiO_2 (wt %) diagram showing the large isotopic variations between the low SiO_2 members of each group and the small differences between the basic to intermediate intrusives located in groups 1–3.

PETROGENESIS OF THE SOUTHERN COASTAL BATHOLITH OF PERU

Recent petrological and geochemical studies supported by detailed mapping of the northern and central segments of the Peruvian Coastal Batholith [*Mukasa*, 1986*a*, *b*; *Pitcher*,

TABLE 5. Isotopic and Trace Element Data for Representative Samples of the Exposed Precambrian Rocks Forming Part of the Arequipa Massif

	Trace Elements, ppm								Isotopic Ratios or Values		
Sample	Rb	Sr	Sm	Nd	Rb/Sr	Sm/Nd	La/Yb	Th/U	ε_{Sr_p}	ε_{Nd_p}	$^{206}Pb/^{204}Pb_p$
Mollendo Granulites											
PE-18	88	97	4.61	26.3	0.91	0.18	54.7	70.0	+999	n.d.	16.110
PE-19	61	160	5.58	34.6	0.38	0.16	>57	70.0	+538	−29.5	16.008
Charcani Gneiss											
PE-37	112	221	8.73	45.8	0.50	0.19	29.0	19.5	+396	−21.4	16.940
PE-111	124	287	9.05	46.8	0.43	0.19	14.1	21.9	+474	n.d.	17.029

Sr isotopic data are from *James et al.* [1976] and Pb isotopic data from *Tilton and Barreiro* [1980]; n.d., no data; p, present day.

1985; *Moore*, 1984; *Atherton et al.*, 1979] have helped to establish fairly comprehensive petrogenetic models concerning its origin and evolution. Most models now recognize the predominant role of fractional crystallization in deriving the granodioritic to monzogranitic plutons from gabbroic and dioritic magmas. Modeling with major and trace element data can generally predict the observed chemical variations inside each superunit by the separation of the modal mineral assemblage; namely plagioclase, hornblende, biotite, K-feldspar, and pyroxene. This is especially evident for the best investigated sections such as in the Tiabaya superunit [*Atherton and Sanderson*, 1985] or in the Linga-Arequipa superunit [*LeBel*, 1985].

Isotopic studies also reveal that when the Coastal Batholith was emplaced in a marginal basin, thus away from the influence of an old continental crust (i.e., the Lima and Trujillo segments [*Atherton et al.*, 1983]), the early gabbroic rocks and the mafic-intermediate plutons belonging to the Late Cretaceous superunits carry Sr and Pb isotopic compositions slightly higher to those generally ascribed by subcontinental mantle values [see *Beckinsale et al.*, 1985; *Mukasa*, 1986*a*]. This would suggest that (1) the source of the Coastal Batholith is basic to ultrabasic in composition and (2) it ultimately resides in the mantle wedge above the subduction zone and/or in the lower Andean crust having mantlelike isotopic characteristics.

Except for the Tiabaya superunit exposed near Arequipa, the sampling of the other superunits was too regional in scope to allow the clear assessment of the role of fractional crystallization in the formation of the evolved intrusives (granodiorites to monzogranites) from more basic-intermediate compositions (gabbros to diorites). However, if we take into consideration the major and trace element variations portrayed by numerous chemical plots and the mineralogical assemblage of the southern Peruvian intrusives, which is similar to the assemblages observed in many plutonic suites of the Arequipa, Lima, and Trujillo segments, we may reasonably assume that part of the chemical evolution of the southern Peruvian Coastal Batholith can be explained by such a process.

However, what singularizes the chemical evolution of the southern Arequipa and Toquepala segments is the importance of crustal assimilation processes. At least the Nd, Sr, and Pb isotopic data presented here seem to indicate clearly that some assimilation of the Precambrian crust accompanied fractional crystallization. However, the trace element and isotopic data can also be used as a basis for elaborating complex models involving multiple crustal or mantle sources with depleted to enriched isotopic compositions and/or for a more complicated assimilation history implicating both juvenile and old enriched crustal materials. Therefore, in order to explain the evolution of the Coastal Batholith of southern Peru, we must consider at least three petrogenetic models:

Model 1. The chemical and isotopic variations seen in the three groups which are well illustrated by the correlation of the Nd and Sr isotopic enrichment (and $^{206}Pb/^{204}Pb$ depletion) with the density of Precambrian outcrops can be best explained by various amounts of assimilation of Precambrian crustal during fractional crystallization of isotopically homogenous basic parental magmas initially produced through partial melting of the depleted mantle wedge above the subduction zone.

Model 2. The fractionating parental magmas still originate from the mantle wedge. However, during their ascent in the Andean crust, they assimilate roughly the same amount of crustal material with different chemical compositions; one type being characterized by very high ε_{Sr}, low ε_{Nd}, and $^{206}Pb/^{204}Pb$ values and a strong LILE enrichment (i.e., the Precambrian crust, see Table 5), the other being less enriched in Nd and Sr isotopes and with higher $^{206}Pb/^{204}Pb$ ratios (i.e., young underplated crust or mafic crust generated in a prior magmatic event?).

Model 3. A more complex magmatic history involves mixing and fractionation of parental magmas coming from the mafic-ultramafic lower crust and the mantle wedge, both having a range of isotopic compositions from depleted to slightly enriched in Nd, Sr, and Pb isotopes. Upon fractionation and ascent in the Andean crust they would, as in model 2, assimilate various amounts of crustal materials characterized by a wide range of isotopic and trace element compositions.

It may be a priori difficult to choose between these three models, let alone establish quantitative assessments of models 2 or 3. For instance, if model 1 is valid, then we must explain why the intrusives lying in the Ilo-Moquegua transect apparently exhibit little evidence of crustal contamination despite the presence of a thick (>15 km?) Precambrian basement presumably underlying the axis of the Coastal Batholith. Model 1 can at least be evaluated since we already know that some assimilation of a crustal material whose composition is similar to that of the exposed Precambrian crust did take place. Furthermore, we have a good estimate of the trace element and isotopic composition of the mantle wedge above subduction zones from geochemical studies of basalts and andesites erupted in oceanic and continental arcs [see *Gill*, 1981]. We can thereof establish a general quantitative AFC model (i.e., assimilation-fractional crystallization) based upon the available Nd and Sr isotopic

TABLE 6*a*. AFC Model: Nd and Sr Isotopic Values With Selected Trace Element Concentrations Generated in the LPC (Lower Precambrian Crust) Stage

	Initial Magma	Contaminant (Precambrian Crust)	r = 0.1 (Calculated)	Group 1 (Observed)	r = 0.2 (Calculated)	Group 2 (Observed)	r = 0.45 (Calculated)	Group 3 (Observed)	D^*
				Trace Element, ppm					
La	3	63	7.0	8–12	10.6	14–16	25.1	20	0.08
Nd	8	46	12.7	9–18	15.2	16–21	25.1	22	0.2
Sm	2	8.8	3.0	2.1–3.0	3.5	3.9–48	5.8	4.5	0.2
Yb	1	3	1.25	1.4–2.0	1.40	1.9–2.2	2.25	1.9	0.25
Rb	20	120	34	8–23	41	34–95	70	44	0.02
Sr	400	250	519	342–471	524	288–513	550	579	0.3
Zr	66	239	103	64–112	117	67–178	173	53	0.06
Ba	300	1700	489	224–518	585	256–698	973	...	0.15
Th	0.5	15	1.4	1–2	2.3	4–12	5.9	4	0.01
U	0.4	0.7	0.6	0.3–0.6	0.6	0.9–1.6	0.8	1.0	0.01
				Isotopes					
ε_{Sr_i}	−10	+396	−1.2	−7.4 to −1.9	+3.1	+7.7+14.9	+48.5	+19.6	
ε_{Nd_i}	+8	−21	+2.9	+2.2 to +1.7	−1.0	+0.5 to −1.2	−9.4	−4.4	

Mineral assemblage: olivine 30%; clinopyroxene (+ orthopyroxene), 60%; calcic plagioclase, 10%. F = 1.0–0.7. We have used two end-members: (1) a typical parental basic magma formed in the mantle wedge above subduction zones and (2) the exposed Precambrian crust representing the upper crustal contaminant. It is postulated that the mantle wedge was enriched in LILE (and probably L,REE) through plate fluxing/melting or mantle scavenging shortly prior to the melting events. We thus produce parental magmas enriched in LILE but with positive ε_{Nd} and negative or slightly positive ε_{Sr} values (see discussion by *Gill* [1981, chapter 9]). F represents the amount of liquid remaining, r (the r value) the rate of assimilation, and D^* the bulk distribution coefficient (see text). Distribution coefficients for each mineral are taken from a compilation made by *Gill* [1981] and *Boily* [1981].

analyses and try to extrapolate it for some of the trace element data. The principal equations used in this model are given by *DePaolo* [1981*a*, *b*] and *Farmer and DePaolo* [1983].

THE AFC MODEL

We have considered a simple model in which the Nd and Sr isotopic and some of the trace element variations resulted from the interaction of two distinct components: (1) a typical calc-alkaline basic parental magma generated in the mantle wedge above the subduction zone and (2) a Precambrian continental crust such as exposed in the studied area. The trace element and isotopic composition of each end-member is given in Table 6*a*. The crustal end-member (here the contaminant) obviously represents only a fraction of the total Andean continental crust through which the magmas ascended. In view of the complex crustal layering of the Andean crust, it is most likely that magmas coming from the subduction zone also assimilated other types of crustal materials such as the thick mafic crustal root presumably underlying the Precambrian basement [*Jones*, 1981; *Couch et al.*, 1981]. Even if the low $^{206}Pb/^{204}Pb$ ratios recorded by *Tilton and Barreiro* [1980] imply that the gneiss outcropping in the area underwent granulitic metamorphism during the Precambrian (2 Ga [*Daylmayrac et al.*, 1977]), the elevated incompatible trace element content (i.e., Ba, La, Nd, Rb, and Th), fractionated La/Yb and Rb/Sr ratios, and high ε_{Sr_p} values shown by the Charcani gneiss signify that they are too

TABLE 6*b*. AFC Model: Nd and Sr Isotopic Data and Selected Trace Element Concentrations Generated in the MUPC (Middle Upper Precambrian Crust) Stage

	(LPC) r = 0.1 (MUPC) r = 0.05 (Calculated)	Group 1 (Observed)	(LPC) r = 0.2 (MUPC) r = 0.05 (Calculated)	Group 2 (Observed)	(LPC) r = 0.45 (MUPC) r = 0.05 (Calculated)	Group 3 (Observed)	D^*
			Trace Element, ppm				
La	8–18	14–26	12–25	15–30	29–56	22–32	0.2–0.3
Nd	14–25	16–27	26–30	15–27	27–48	16–20	0.25–0.4
Sm	3.3–5.5	3.4–6.0	3.8–6.2	2.7–6.3	5.8–9.3	2.9–3.7	0.3–0.45
Yb	1.3–1.8	1.4–3.1	1.5–2.0	1.4–2.7	2.3–3.0	0.9–1.3	0.5–1.0
Rb	36–68	49–150	43–80	40–290	74–132	72–145	0.3
Sr	538–165	533–292	544–168	526–241	570–175	474–98	0.5–2.5
Zr	104–113	71–239	118–126	63–254	174–182	76–135	0.6–1.0
Ba	521–899	101–722	622–1055	549–1973	1030–1692	550–924	0.3–0.6
Th	1.6–4.2	3–17	2.5–6.5	5–44	6.4–14.1	9–14	0.1
U	0.7–1.4	0.8–5.0	0.7–1.5	1.0–10.3	0.9–1.9	0.9–2.5	0.1
			Isotopes				
$\varepsilon_{Sr\,i}$	−0.5 to +17.4	−4.0 to +3.7	+3.8 to +21.4	+7.1 to +55.7	−49.1 to +63.9	+21.7 to +51.6	
$\varepsilon_{Nd\,i}$	+2.8 to +0.6	+2.4 to −1.2	−1.2 to −2.7	−0.8 to −2.2	−9.5 to −10.1	−5.1 to −8.0	

Mineral assemblage: (1) clinopyroxene, 5%; plagioclase, 50%; hornblende, 35%; biotite, 10%; K-feldspar 0%, (2) clinopyroxene 0%; plagioclase, 55%; hornblende, 35%; biotite, 10%, K-feldspar, 5%. Explanations as in Table 6*a*. F = 0.65–0.23.

enriched to represent adequately a lower crustal component. They obviously constitute part of the upper section of the Andean crust. Furthermore, the composition of the sampled Precambrian gneiss may not be representative of the whole Precambrian segment which could be, as in the case of the lower mafic root, more depleted in LILE and less enriched in Nd and Sr isotopes. Therefore the assimilation rate or "r value" given in the model outlined below must be viewed only as a lower estimate of the total rate of crustal assimilation encountered by the incoming magmas. Furthermore, if the latter did assimilate crustal materials presenting similar isotopic compositions, then it would be very hard to detect with radiogenic isotopes alone, but this could nevertheless modify the incompatible trace element content of the evolving magmas.

The AFC model was subdivided in two stages. The first, LPC or Lower Precambrian Crust (LPC), occurs in the lower part of the Precambrian basement and/or at the interface of the mafic Andean root and the base of the Precambrian crust. During this stage, it is assumed that hot and dense mafic magmas rising from the mantle wedge and passing through the mafic root will either stop and start fractionating at the base of the Precambrian basement and/or ascend slowly through this low density slab (i.e., the 2.75 g/cm^3 slab probably representing part of the Arequipa Massif [*Couch et al.*, 1981]). Therefore the magmas must crystallize dense minerals with high heat of fusion (i.e., olivine, orthopyroxene, and clinopyroxene) to reduce their density. This will release heat and promote substantial assimilation of an already hot and readily fusible siliceous crust at depth. Thus, in the LPC stage, we should expect the bulk of assimilation to occur in relatively basic magmas when suites of gabbroic to quartz-dioritic/monzodioritic magmas are derived via fractional crystallization of mineral phases such as olivine, clinopyroxene ± orthopyroxene, and perhaps calcic plagioclase.

The second stage, (MUPC) or Middle Upper Precambrian Crust, will generate suites of monzodiorite/quartz-diorite to tonalite/granodiorite-monzogranite plutons derived from the residual magmas left from the LPC stage when they rise, differentiate, and crystallize to high crustal levels. During this stage, we assume that the amount of assimilation will generally decrease since the temperature contrast between magma and wall rock becomes less important, the former being less hot and more viscous than during the LPC stage. The fractionating mineral assemblage will be formed by plagioclase, amphibole, biotite, and K-feldspar with minor participation of clinopyroxene, magnetite, and, in the later stages, accessory phases (zircon, apatite, sphene, etc.).

The salient results of the AFC model are illustrated in Figures 7 and 8 and presented in Tables 6*a* and 6*b*. The important parameter to consider is r (or r value) which gives the assimilation rate equal to M_a/M_c, where M_a represents the rate of wall rock assimilation (mass/unit time) and M_c is the rate at which the fractionating mineral phases are being effectively separated from the magma [*DePaolo*, 1981*a*]. The results of the model are especially well illustrated in the trace element-isotope plots (Figures 7 and 8). They show that less than 30% crystallization of the parental magmas (F = 0.9–0.7) is needed to generate the observed isotopic variations when the r value varies from 0.1 to 0.45 in the LPC stage. For group 1, which includes all plutons lying in the Ilo-Moquegua transect, the r value remains fixed around 0.1

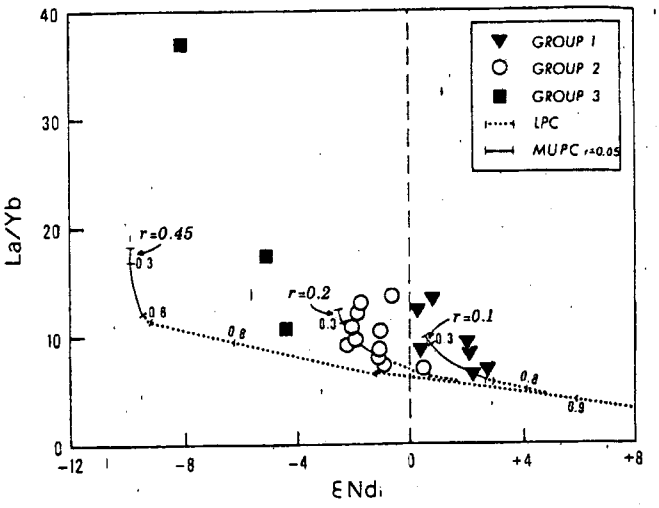

Fig. 7. AFC model. La/Yb versus $\varepsilon_{Nd\ i}$ plot showing three contamination lines generated by our AFC model. LPC, Lower Precambrian Crustal stage; MUPC, Middle Upper Precambrian Crustal stage; r, rate of assimilation; r (the r value) is given by M_a/M_c, where M_a is the rate at which a magma is assimilating wall rock and M_c is the rate at which the fractionating minerals are being effectively removed from the magmas [see *DePaolo*, 1981*a*]. The r value is fixed at 0.05 in the MUPC stage. Tick marks on each contamination line represent F; the amount of remaining liquid after separation of the mineral phases for which the proportions are given in Tables 6*a* and 6*b* (see text).

and increases slightly to 0.2 for group 2. Only for group 3, the Linga-Yarabamba plutons lying adjacent to Precambrian outcrops, did the r value reach 0.3–0.45. In this stage, La and Yb are incompatible elements ($D^* < 0.3$) and the contamination lines run almost parallel to the $\varepsilon_{Nd\ i}$ axis (Figure 7). In fact, if we assume a fixed interval of crystallization (F = 0.7), then for r values progressing from 0.1 to 0.45, the $\varepsilon_{Nd\ i}$ values increase substantially from +3 to −9 (12 ε units), the La/Yb ratios vary from 6 to 12, and the Nd concentrations change from 12 to 25 ppm. Thus for the LPC stage, the AFC model is well able to reproduce the large isotopic as well as trace element differences observed between the basic-intermediate plutons of each group (i.e., quartz-gabbro to monzodiorite, see also Figure 6).

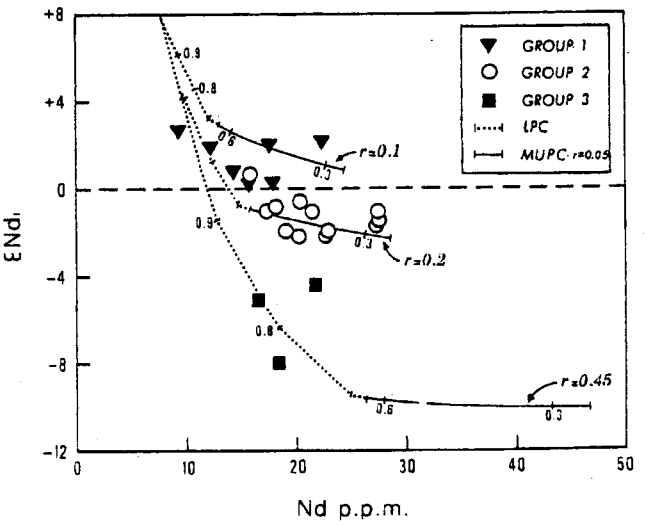

Fig. 8. AFC model. $\varepsilon_{Nd\ i}$ versus Nd (ppm). Explanations as in Figure 7.

The MUPC stage brings about a drastic change in the contamination trend. The r value must remain close to 0.05 during the fractionation interval (F = 0.7–0.25) needed to generate the quartz-monzodiorite to tonalite/granodiorite to monzogranite suites. The contamination lines become steeper in the La/Yb versus $\varepsilon_{Nd\,i}$ plot (Figure 7) while they tend to flatten in the $\varepsilon_{Nd\,i}$ versus Nd (ppm) plot (Figure 8). Due to extensive plagioclase and hornblende/biotite fractionation, Sr becomes compatible at this stage, and the rest of the considered trace elements including Yb follow in becoming less incompatible. For this reason, the La/Yb ratios increase sharply but due to low r values, the $\varepsilon_{Nd\,i}$ values vary little as opposed to the LPC stage. Again, this supports our assumption that minimal contamination in the MUPC stage follows extensive fractional crystallization, a process which will ultimately enrich the residual magmas in incompatible trace elements but will bring little change in its isotopic composition.

Tables 6*a* and 6*b* also compares the results obtained by the AFC model with the observed data. While the predicted isotopic data seem to match the observed data in the MUPC stage, the model overestimates the Ba and REE abundances, while it underestimates the concentrations in Th and U. This may reflect the inherent oversimplification of the model and the fact that the more evolved plutons are dominated by granodiorites instead of monzogranites. This would in fact reduce the required degree of crystallization needed to produce less siliceous compositions and therefore lower the predicted concentrations in incompatible elements. Also, as proposed in models 2 and 3, there may be more than one contaminant involved with compositions far less enriched in LILE and with lower ε_{Sr} and higher ε_{Nd} values than what is actually shown by the exposed basement rocks, even if they are of Precambrian age. Finally, the intrusive suites of each superunit may have evolved from parental magmas with slightly different trace element signatures and fractionated mineral phases in different proportions, although they may have followed the same differentiation path.

Although we recognized that this AFC model may be too crude in its details, one conclusion stems out of this exercise. When considering the entire Coastal Batholith of southern Peru, the required amount of crustal assimilation needed to match the observed isotopic, and to a lesser extent, the trace element signatures is surprisingly low considering the omnious presence of an exposed basement which is characterized by such a distinct chemical and isotopic composition (Table 5). Moreover, the assumption that we have only one crustal contaminant involved (i.e., the Precambrian crust) has some credibility. The most compelling argument is certainly the fact that all post-Oligocene ignimbrites and andesites which erupted in southern Peru, including those lying in the Ilo-Moquegua transect at proximity of the Coastal Batholith, were far more contaminated than the Jurassic to Paleocene intrusives [*Barreiro and Clark*, 1984; *James*, 1981; M. Boily et al., submitted manuscript, 1989]. In these studies, all post-Oligocene ignimbrites and andesites show elevated La/Yb ratios (>14) and $\varepsilon_{Sr\,i}$ values (> +13), low $\varepsilon_{Nd\,i}$ values (< −1.0) and $^{206}Pb/^{204}Pb$ ratios (<18.207) that can also be generated by an AFC process with the Precambrian crust acting as a contaminant. Thus we strongly suspect that a Precambrian basement having a large granulitic component underlain the axis of the Coastal Batholith during its formation, although we are aware of a 35-m.y. gap between the last intrusive pulse and the first eruption of post-Oligocene ignimbrites. Finally, we also believe that the three petrogenetic models proposed earlier are all plausible, although we would tend to favor model 1 for its simplicity and ability to test it. However, we acknowledge the inherent limitations of such an exercise, since we can only identify one contaminant and used only one homogenous mantle source.

DISCUSSION

An Extensional Marginal Basin in Southern Peru?

During the Mesozoic era, extensional marginal basins were formed in Peru and southern Chile during or shortly prior to the emplacement of the Coastal Batholith. In central Peru, the marginal basin and Coastal Batholith axes are underlain by a large archlike structure of dense rocks (3.0 g/cm^3) variously interpreted as imbricated upthrusts of oceanic crust, intrusions at depth, or upper mantle upwelling during subduction which could all indicate crustal rupture [*Atherton et al.*, 1983]. This structure is absent in the area of study (16°–18°S) and is replaced by a thick (10–15 km) low-density crustal slab (2.75 g/cm^3) probably representing a section of the Precambrian-Paleozoic craton. It is possible that in southern Peru, the thickness of the Precambrian basement may have been substantially increased by tectonic processes during the Tertiary, perhaps by repeated underthrusting [see *Suarez et al.*, 1983], and thus may have been be much thinner during the Mesozoic. However, the limited amount of crustal assimilation experienced by the Coastal Batholith (see AFC model) would suggest, as one possibility, that the Mesozoic Andean crust of southern Peru must have somehow reacted to the same extensional stress that affected central Peru. The Andean crust, at least in this transect, may have been stretched, thinned, and possibly partially disrupted. Crustal disruption may not have been as important as in central Peru, and the extensional structures could have been obliterated partly by the strong post-Cretaceous tectonic events that led to uplift, crustal thickening, and horizontal shortening in southern Peru [*Suarez et al.*, 1983; *Audeband et al.*, 1973].

Crustal extension and thinning could explain the limited amount of contamination experienced by the Jurassic-Paleocene southern Peruvian plutons relative to the post-Oligocene volcanics. Thinning of the Andean crust would allow large volumes of basic magmas to encounter the Precambrian crust at shallower depth, perhaps 5–10 km, where the ambiant crustal temperatures would be much lower than what prevails at 20–25 km (the actual depth of the low-density slab). This would impede large-scale assimilation in part due to a larger temperature contrast between crust and magma. This conclusion is consistent with *DePaolo*'s [1981*b*] contention that the zone of extensive crustal assimilation (large r values) is located at crustal depths below 15 km.

The observed Nd, Sr, and Pb isotopic variations and their definite correlation to the density of Precambrian outcrops may then indicate that the basement was more distended in the Ilo-Moquegua transect relative to the Arequipa and Tacna regions, thus allowing the magma bodies to rise and differentiate at even shallower crustal depth and limiting the amount of assimilation in the first case. We may speculate that a thinner crust in this transect may have promoted the

development of basinal structures in which sediments were later deposited and also facilitated the extrusion of large volumes of volcanic rocks that may now cover the basement rocks. It is revealing that the Jurassic and Late Cretaceous to early Paleocene volcanics (Chocolate Formation and Toquepala Group), also showing positive $\varepsilon_{Nd\ i}$ and negative $\varepsilon_{Sr\ i}$ values, were erupted largely in the Ilo-Moquegua transect [*Boily et al.*, 1984]. Conversely, the whole region may have been subjected to the same extensional stress, but the Ilo-Moquegua transect had originally a thinner crust.

The absence of geological features associated to extensional tectonics such as those observed in the northern marginal basin (i.e., series of normal faults parallel to the oceanic trench, numerous dyke swarms) obviously underlines the major weakness of this hypothesis, although some of these features may be buried under the extensive Mesozoic-Recent volcano-sedimentary cover.

As an alternative explanation, we can assume that if during Coastal Batholith formation, large volumes of basic magmas were injected into the Andean crust, then its bulk composition will reflect a mixture of mantle derived magmas and mafic cumulates that digested a substantial amount of preexisting crust. Repeated mantle intrusions could reduce the importance of the Precambrian component and create a lower and middle crustal segments with isotopic characteristics intermediate between crust and mantle [see *Farmer and DePaolo*, 1983]. Thus the apparent low rate of assimilation (r value = 0.1–0.45) needed to produce the isotopic and trace element variations in the LPC stage may be misleading, as this "new" crustal composition would permit a substantial increase in the r value.

Finally, as proposed in models 2 and 3, the Coastal Batholith may have assimilated a younger less enriched crust underlying the Ilo-Moquegua transect. In this case it would obviate the necessity of thinning and/or breaking the crust. However, we would still have to explain why the southern Peruvian post-Oligocene volcanics, including those erupted in the Ilo-Moquegua transect, assimilated a lot more of Precambrian crustal material than did the Jurassic to Paleocene intrusives (M. Boily et al., submitted manuscript, 1989).

Batholith Formation: A Mantle or Crustal Process?

The close association between subduction, calc-alkaline magmatism, and crustal growth is especially evident along the western Peruvian margin. In southern Peru, since the onset of subduction at the end of the Triassic, large volume of basaltic, andesitic, and rhyolitic (ignimbrite) volcanic rocks erupted in the pre- and western Cordilleras and in the western Altiplano with magmatic gaps between 100–150 Ma and 25–64 Ma [*Tosdal et al.*, 1981; *James et al.*, 1974, 1976). The Coastal Batholith was emplaced in the Andean crust in discrete magmatic pulses from the Late Jurassic to early Paleocene epochs (i.e., 184–190 Ma, 99–111 Ma, and 59–86 Ma [*Beckinsale et al.*, 1985; *Mukasa*, 1986*a*]).

The volume of the Peruvian Coastal Batholith is especially important. Depending on the proposed shape of the Batholith at depth, it is estimated that from 3×10^4 to 1×10^5 km^3 per 1° of latitude of plutonic material was generated in western Peru, implying a rate of production between 2.9 and 9.9×10^{-6} km^3 yr^{-1} per km of plate margin [*Francis and Rundle*, 1976; *Hamilton and Myers*, 1974]. It is difficult to estimate the volume of the entire Coastal Batholith southeast of Arequipa, since not only is the batholith divided in two major sections (instead of being confined to a narrow 50-km strip), but it is also concealed over a large area by Mesozoic to Recent volcanics and sediments. However, if we assume a similar intrusion rate to that proposed for the whole Peruvian Coastal Batholith and a mean density of 2.9 g/cm^3 (gabbroic composition), then we obtain a rate from 8.4×10^6 to 2.9×10^7 kg yr^{-1} per km of plate margin. Over the 230 km of plate margin covered in this study, we estimate that from 1.9 to 6.7×10^9 kg yr^{-1} of plutonic material was emplaced in the crust. If the conclusions of our AFC model are correct, then we can calculate the mass ratio of assimilated crust to the original mantle magmas introduced in the Andean crust upon batholith formation (i.e., $M_a/M_m{}^0$ [*Depaolo and Farmer*, 1983]) and assume that a maximum of 85–95% or $1.6–6.4 \times 10^9$ kg yr^{-1} was originally derived from the mantle wedge above the subduction zone. This assumption is valid if the process of melting or "fluxing" of the downgoing oceanic slab in the subduction zone brings only small changes in the LILE and isotopic compositions of the mantle and does not carry enough "bulk" mass compared to the total mass of mantle wedge involved during batholith formation.

We can estimate the total mass of the mantle wedge above the descending slab and underlying the studied area at the time of Coastal batholith formation; i.e., 230 km of plate length from Arequipa to the Chilean border × 150 km of plate width taken from the Peruvian trench to the eastern extent of the Coastal Batholith. If we allow a 30° subduction angle for the descending oceanic plate, the maximum angle encountered in regions of intense calc-alkaline magmatism in the Andes [*Barazangi and Isacks*, 1976], and a Mesozoic continental crust of 30 km in thickness, then a simple calculation produces a volume of 6.4×10^5 km^3 for the subcontinental mantle trapped between the subduction zone and the base of the crust with a total mass of 2.1×10^{18} kg (density assumed: 3.33 g/cm^3). However, this total mass is reduced to 1.3×10^{18} kg if we only consider the mantle segment underlying the Coastal Batholith. Alternatively, the trapped mantle mass could be greater if Mesozoic extension caused substantial thinning of the Andean crust underlying the Coastal Batholith prior to or during its formation, although it may be difficult to evaluate the effect of this process in this crude calculation. Over a period of 130 m.y., up to 2.1 to 8.3×10^{17} kg of plutonic material would be generated from this mantle. This intrusive mass represents between 16 and 64% of the total estimated mass of the mantle wedge. This is a substantial proportion since, in this calculation, we ignored the mass of volcanic material generated during this 130-m.y. interval. We can even speculate that part of the mantle trapped between the descending plate and the Andean crust is "frozen" at the base of the lithosphere and thus may have been largely infertile due to previous melting events; therefore the total fertile mantle mass may be much lower than our estimate. This could be compensated by a greater mass underlying an Andean crust that was stretched and thinned during the Mesozoic.

On the other hand, if the whole Coastal Batholith has to be entirely generated from the lower mafic-ultramafic Andean crustal root (density: 3.05 g/cm^3) with little participation from the subcontinental mantle, then we could need total melting of a 230 × 150 × 8 km crustal segment or more realistically 25–30 wt % melting of a 230 × 150 × 30 km

crustal section, all depending on the bulk composition of the lower part of the crust.

We can draw simple conclusions from these crude calculations: (1) the lower mafic-ultramafic Andean crust cannot solely generate the total mass of the Coastal Batholith emplaced in southern Peru during the last 130 m.y., (2) that probably some assimilation of the lower crust and/or mixing of lower crustal melts with mantle derived magmas did occur, and (3) a strongly convective mantle which is replenished over 130 m.y. is needed to satisfy the mass requirement for volcanism and plutonism.

CONCLUSIONS

On the basis of major and trace element analyses, each superunit composing the southern segments of the Peruvian Coastal Batholith is formed by distinct suites of typical calc-alkaline plutons that range in composition from quartz gabbro to granodiorite. We also documented that for all plutons, the decrease in $\varepsilon_{Nd\,i}$ and increase in $\varepsilon_{Sr\,i}$ values are accompanied by a substantial lowering of the $^{206}Pb/^{204}Pb_i$ ratios which can be correlated to the density of Precambrian outcrops.

We have suggested three petrogenetic models in order to explain the isotopic and trace element variations portrayed by the intrusives. A simple quantitative AFC model involves the formation of parental basic magmas through partial melting of an homogenous mantle wedge above the subduction zone and different amounts of assimilation of the Precambrian crust (i.e., a small amount in the Ilo Moquegua transect (group 1) and substantially more in the Arequipa and Tarata areas (groups 2 and 3)) when magmas ascend and fractionate at the base and/or in the Precambrian crust. However, despite the continuous presence of a Precambrian basement, the overall rate of assimilation (r value) remains relatively low if we consider the entire southern Peruvian Coastal Batholith. Other more complex models are plausible. Mixing of parental magmas derived both from the mantle and the lower mafic-ultramafic crust with slightly heterogenous but depleted Nd and Sr isotopic signatures could accompany crustal assimilation of different types of Andean crustal material. The first type is formed by a young and perhaps less enriched crust underlying the Ilo-Moquegua transect and the second one, is dominated by an older Precambrian section under the Arequipa and Tarata areas. In all models we recognize the importance of fractional crystallization during the formation of the more evolved plutons of each superunit (i.e., tonalite/granodiorites-monzogranites) from gabbroic and dioritic magmas.

If our simple AFC model is correct, then the relatively small degree of assimilation needed to generate the observed isotopic and trace element variations in the plutons could possibly be explained if the southern Peruvian crust was stretched, thinned, and partially disrupted during the prevailing extensional tectonics that led to the formation of a Mesozoic marginal basin in central Peru. This would allow mantle-derived magmas to encounter the base of the Precambrian basement at shallower depth and/or spend less time differentiating in this enriched crust, thereby greatly reducing the possibility of assimilation. Other interpretations are possible, and we cannot fully support this hypothesis until we have a better understanding of the crustal structure of southern Peru.

Acknowledgments. This paper constitutes part of a Ph.D. thesis undertaken by the senior author at the Université de Montréal. The authors are indebted to J. Patchett, F. Frey, and an anonymous reviewer for their constructive criticisms. We thanked Mona Katchami for the skillfull drafting of many figures.

REFERENCES

Atherton, M. P., and M. L. Sanderson, The chemical variation and evolution of the super-units of the segmented Coastal Batholith, in *Magmatism at a Plate Edge, The Peruvian Andes*, edited by W. S. Pitcher, M. P. Atherton, E. J. Cobbing, and R. D. Beckinsale, pp. 208–227, Blackie, Glasgow, 1985.

Atherton, M. P., W. J. McCourt, L. M. Sanderson, and W. P. Taylor, The geochemical character of the segmented Peruvian Coastal Batholith and associated volcanics, in *Origin of Granite Batholiths: Geochemical Evidence*, edited by M. P. Atherton and J. Tarney, pp. 45–64, Shiva, Cambridge, Mass., 1979.

Atherton, M. P., W. S. Pitcher, and V. Warden, The Mesozoic marginal basin of central Peru, *Nature*, *305*, 3030–3036, 1983.

Audeband, E., R. Capdevilla, B. Daylmayrac, J. DeBelmas, G. Laubacher, C. Lefèvre, R. Marocco, C. Martinez, M. Mattauer, R. Mégard, J. Paredes, and P. Tomasi, Les traits essentiels des Andes centrales (Pérou-Bolivie), *Rev. Geogr. Phys. Géol. Dyn.*, *15*(1-2), 73–114. 1973.

Barazangi, M., and B. L. Isacks, Spatial distribution of earthquakes and subduction of the Nazca plate beneath South America, *Geology*, *4*, 686–692, 1976.

Barreiro, B. A., and A. H. Clark, Lead Isotopic evidence for evolutionary changes in magma-crust interaction, Central Andes, southern Peru, *Earth Planet. Sci. Lett.*, *69*, 30–42, 1984.

Beckinsale, R. D., A. W. Sanchez-Fernandez, M. Brook, E. J. Cobbing, W. P. Taylor, and D. Moore, Rb-Sr whole-rock isochrons and K-Ar age determinations for the Coastal Batholith of Peru, in *Magmatism at a Plate Edge, The Peruvian Andes*, edited by W. S. Pitcher, M. P. Atherton, E. J. Cobbing, and R. D. Beckinsale, pp. 117–202, Blackie, Glasgow, 1985.

Boily, M., Les basaltes de la ceinture métavolcanique archéenne de l'Abitibi et les basaltes modernes: une étude géochimique comparative, MsC. thesis, 142 pp., Univ. de Montréal, Montreal, Que., 1981.

Boily, M., C. Brooks, and D. E. James, Geochemical characteristics of the late Mesozoic Andean Volcanics, in *Andean Magmatism: Chemical and Isotopic Constraints*, edited by R. S. Harmon and B. A. Barreiro, pp. 190–202, Shiva, Cambridge, Mass., 1984.

Chauvel, C., B. Dupré, and G. A. Jenner, The Sm-Nd age of Kambalda volcanics is 500 Ma too old, *Earth Planet. Sci. Lett.*, *74*, 315–324, 1985.

Cobbing, E. J., and W. S. Pitcher, Andean plutonism in Peru and its relationship to volcanism and metallogenesis at a segmented edge, *Mem. Geol. Soc. Am.*, *159*, 277–291, 1983.

Cobbing, E. J., W. S. Pitcher, and W. P. Taylor, Segments and super-units in the Coastal Batholith of Peru, *J. Geol.*, *85*, 625–631, 1977.

Couch, R., R. Whitsett, B. Huehn, and L. Briceno-Guarpe, Structures of the continental margin of Peru and Chile, Nazca Plate: Crustal Formation and Andean Convergence, edited by L. D. Kulm, J. Dymond, E. J. Dasch, and D. M. Hussong, *Mem. Geol. Soc. Am.*, *154*, 703–726, 1981.

Daylmayrac, B., J. R. Lancelot, and A. Leyreloup, Evidence of 2 b.y. old granulites in the late Precambrain metamorphic basement rocks along the southern Peruvian Coast, *Science*, *198*, 49–51, 1977.

DePaolo, D. J., Trace element and isotopic effects of combined wallrock assimilation and fractional crystallization, *Earth Planet. Sci. Lett.*, *53*, 189–202, 1981*a*.

DePaolo, D. J., A neodymium and strontium isotopic study of the Mesozoic calc-alkaline granitic batholiths of the Sierra Nevada and Peninsular Ranges, California, *J. Geophys. Res.*, *86*, 10,470–10,488, 1981*b*.

Farmer, G. L., and D. J. DePaolo, Origin of Mesozoic and Tertiary granites in the western United States and implications for the pre-Mesozoic crustal structure, 1, Nd and Sr isotopic studies in the geocline of the northern Great Basin, *J. Geophys. Res.*, *88*, 3379–3401, 1983.

Francis, P. W., and C. C. Rundle, Rates of production of the main

magma types in the central Andes, *Geol. Soc. Am. Bull., 87*, 474–480, 1976.

Garcia, W., Geologia de los Cuadrangulos de Mollendo y La Joya, *Bol. Serv. Geol. Minas Lima, 19*, 93 pp., 1968.

Gill, J. B., *Orogenic Andesites and Plate Tectonics*, 390 pp., Springer-Verlag, New York, 1981.

Hamilton, W., and W. B. Myers, Nature of the Boulder Batholith of Montana, *Geol. Soc. Am. Bull., 85*, 365–378, 1974.

Hart, S. R., and C. Brooks, The geochemistry and evolution of early Precambrian mantle, *Contrib. Mineral. Petrol., 61*, 109–128, 1977.

Irvine, T. N., and W. R. A. Baragar, A guide to the chemical classification of the common volcanic rocks, *Can. J. Earth Sci., 8*, 523–548, 1971.

James, D. E., A combined O, Sr, Nd and Pb isotopic and trace element study of crustal contamination in central Andean lavas, 1, Local geochemical variations, *Earth Planet. Sci. Lett., 57*, 47–62, 1981.

James, D. E., C. E. Brooks, and A. Cuyubamba, Strontium isotopic composition and K, Rb, Sr geochemistry of Mesozoic volcanic rocks of the Central Andes, *Year Book Carnegie Inst. Washington, 73*, 970–983, 1974.

James, D. E., C. E. Brooks, and A. Cuyubamba, Andean Cenozoic volcanism: Magma genesis in light of strontium isotopic composition and trace element geochemistry, *Geol. Soc. Am. Bull., 87*, 592–600, 1976.

Jones, P. R., Crustal structure of the Peru continental margin and adjacent Nazca plate 9°S latitude, Nazca Plate: Crustal Formation and Andean Convergence, edited by L. D. Kulm, J. Dymond, E. J. Dasch, and D. M. Hussong, *Mem. Geol. Soc. Am., 154*, 423–443, 1981.

Lee, L. M., Mineralization in the Arequipa segment: The porphyry-Cu deposit of Cerro Verde/Santa Rosa, in *Magmatism at a Plate Edge, The Peruvian Andes*, edited by W. S. Pitcher, M. P. Atherton, E. J. Cobbing, and R. D. Beckinsale, pp. 250–260, Blackie, Glasgow, 1985.

LeMaître, R. W., Some problems of the projection of chemical data into mineralogical classification, *Contrib. Mineral. Petrol., 56*, 181–189, 1976.

Lopez-Escobar, L., F. A. Frey, and M. Vergara, Petrogenesis of the Tertiary granitoïds of southern Chile (33°S–34°S), *Contrib. Mineral. Petrol., 70*, 439–450, 1979.

McCourt, W. J., The geochemistry and petrography of the Coastal Batholith of Peru, Lima segment, *J. Geol. Soc. London, 138*, 407–420, 1981.

Moore, N. D., Potassium-argon ages from the Arequipa segment of the Coastal Batholith and their correlation with regional tectonic events, *J. Geol. Soc. London, 141*, 511–519, 1984.

Mukasa, S. M., Common Pb isotopic compositions of the Lima, Arequipa and Toquepala segments in the Coastal Batholith, Peru: Implications of magmagenesis, *Geochim. Cosmochim. Acta, 50*, 771–782, 1986*a*.

Mukasa, S. M., Zircon U-Pb ages of super-units in the Coastal Batholith, Peru: Implications for magmatic and tectonic processes, *Geol. Soc. Am. Bull., 97*, 241–254, 1986*b*.

Norrich, K., and J. T. Hutton, An accurate X-ray spectrographic method for the analysis of a wide range of geological samples, *Geochim. Cosmochim. Acta, 33*, 431–453, 1969.

Pitcher, W. S., A multiple and composite batholith, in *Magmatism at a Plate Edge, The Peruvian Andes*, edited by W. S. Pitcher, M. P. Atherton, E. J. Cobbing, and R. D. Beckinsale, pp. 93–101, Blackie, Glasgow, 1985.

Shackleton, R. M., A. C. Ries, M. P. Coward, and P. R. Cobbold, Structure, metamorphism and geochronology of the Arequipa Massif of Coastal Peru, *J. Geol. Soc. London, 136*, 195–294, 1979.

Stewart, J. W., J. F. Evernden, and N. J. Snelling, Age Determinations from Andean Peru: A reconnaissance survey, *Geol. Soc. Am. Bull., 85*, 1107–1116, 1974.

Suárez, G., P. Molnar, and B. C. Burchfiel, Seismicity, fault plane solutions, depth of faulting and active tectonics of the Andes of Peru, Ecuadore, and southern Colombia, *J. Geophys. Res., 88*, 10,403–10,428, 1983.

Tilton, G. R., and B. A. Barreiro, Origin of lead in Andean calc-alkaline lavas, southern Peru, *Science, 210*, 1245–1247, 1980.

Tosdal, R. M., E Farrar, and A. H. Clark, K-Ar geochronology of the late Cenozoic volcanic rocks of the Cordillera Occidental, southernmost Peru, *J. Volcanol. Geotherm., Res., 10*, 157–173, 1981.

Wasserburg, G. J., S. B. Jacobsen, D. J. DePaolo, M. T. McCulloch, and T. Wen, Precise determination of Sm/Nd ratios, Sm and Nd isotopic abundances in standard solutions, *Geochim. Cosmochim. Acta, 45*, 2311–2323, 1981.

Zindler, A., S. R. Hart, and F. A. Frey, Nd and Sr isotopes ratios and rare earth element abundances in Reykjanes Peninsula basalts: Evidence for mantle heterogeneity beneath Iceland, *Earth Planet. Sci. Lett., 45*, 249–262, 1979.

M. Boily, IREM-MERI, Ecole Polytechnique, C. P. 6079, Succ "A," Montréal, Quebec, Canada H3C 3A7.

C. Brooks and J. N. Ludden, Département de Géologie, Université de Montréal, C. P. 6128, Succ "A," Montréal, Quebec, Canada H3C 3J7.

D. E. James, Carnegie Institution of Washington, Department of Terrestrial Magnetism, 5241 Broad Branch Road, NW, Washington, DC 20015.

(Received October 21, 1987;
revised November 30, 1988;
accepted April 10, 1989.)